Available online at www.sciencedirect.com
SCIENCE DIRECT®
ELSEVIER
Nuclear Instruments and Methods in Physics Research B 200 (2003) 148–154
NIM B
Beam Interactions with Materials & Atoms
www.elsevier.com/locate/nimb

Characterisation of new hybrid organic–inorganic nickel silicates by polarised EXAFS

Mireille Richard-Plouet [a,*], Murielle Guillot [a], Agnès Traverse [b], Daniel Chateigner [c], Serge Vilminot [a]

[a] GMI-IPCMS UMR-CNRS 7504 23, rue du Loess, F-67037 Strasbourg, France
[b] LURE BP 34, F-91898 Orsay Cedex, France
[c] CRISMAT-ISMRA, UMR-CNRS 6508, bd. M. Juin, F-14050 Caen, France

Abstract

The angular dependence of the X-ray absorption coefficient (P-EXAFS) has been used in order to characterise the local order, around the metallic cation, in two lamellar nickel silicates, with Ni/Si = 3/2 or 3/1. The aim of this study is to get insight into the local environment of Ni^{2+} cations concerning the first and second shells. The first neighbours are oxygen in octahedral arrangement, with a flattening angle of 59° or 60° for the two studied compounds. The second shell consists in 6 Ni, as expected for trioctahedral hydroxide layer and 2 Si grafted to the layer. From the evolution of Si coordination with the incident angle of the X-ray beam, Si are grafted with a random orientation and not only rigorously perpendicularly to the layers, as can be observed in clay materials.

PACS: 61.10.H; 68.55.J; 81.20.F; 61.46
Keywords: Polarised EXAFS; Organic–inorganic silicates; Texture; Hydrothermal treatment

1. Introduction

In addition to their possible applications as ion absorption [1,2], organo-modified phyllosilicates are promising materials for in situ intermolecular reactions with guest species [1,3,4]. Usually, these materials are obtained by precipitation with sodium hydroxide near room temperature, starting from divalent cation chloride and selected organo-modified Si alkoxides. The structure is supposed to be based on a clay arrangement, i.e. brucite like layers (M^{II} in octahedral sites sharing edges) to which hexagonal rings consisting of Si tetrahedra sharing corners are connected [3,5,6]. This hypothesis has not yet been supported by experimental features, since the obtained solids are poorly crystallised and powder diffraction data are too poor to allow a structural model refinement. We recently investigated the possibility to obtain these phases by hydrothermal treatment under autogenous pressure instead of precipitation [7,8]. The crystallinity was marginally improved and several characterisations were carried out. If the grafting of the silicate species was demonstrated in

* Corresponding author. Tel.: +33-3-88-107129; fax: +33-3-88-107247.
E-mail address: richard@ipcms.u-strasbg.fr (M. Richard-Plouet).

0168-583X/02/$ - see front matter
PII: S0168-583X(02)01711-1

particular through XAS at the Ni K-edge, no information on the Ni–O–Si bond direction or the condensation of the silicate tetrahedra could be evidenced. A. Manceau et al. [9–12] have recently demonstrated the ability of polarised EXAFS (P-EXAFS) to get structural information from self supporting clay films. Our study focuses on the P-EXAFS and quantitative texture analysis (QTA) of hydrothermally synthesised nickel aminopropyl modified silicate films. Two films deposited on amorphous substrates with a cationic ratio Ni/Si of 3/2 (**S20**) and 3/1 (**S50**) are studied, which exhibit different, low temperature, magnetic ordering: ferromagnetic and canted antiferromagnetic respectively. Our aim is to check, first of all, if the organo-modified silicates are connected to the layers as in clays and secondly, if in these two phases, Ni^{2+} cations present the same environment and are magnetically coupled similarly inside the layers.

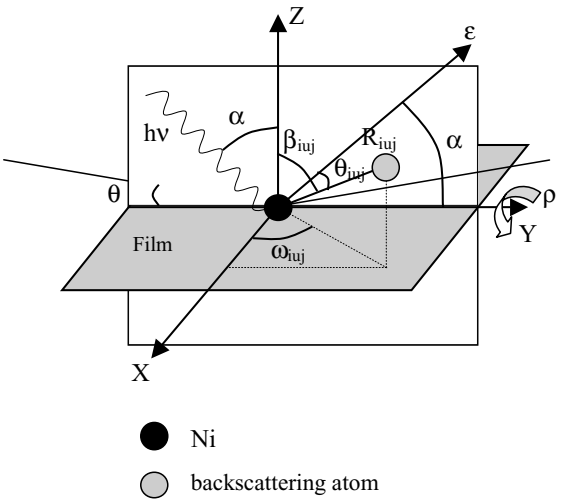

Fig. 1. Coordinate system for angular measurements on self-supported films.

2. Experimental

2.1. Synthesis

The studied silicates are obtained according to conditions already reported [7,8]. Oriented films were prepared by dispersion of the silicate in decarbonated water in order to obtain a colloidal suspension. Upon settling and slow drying at room temperature, crystallites are deposited either onto glass slides or kapton for texture and X-Ray absorption measurements respectively, with the layer stacking axis perpendicular to the substrate.

2.2. Texture measurements

QTA was performed, at the incident angle of the (0 0 5) line (2θ close to 10°, wavelength Cu $K_{\alpha 12}$). For this position, all the diffracted peaks in the 10–95° 2θ range are recorded simultaneously using a curved position sensitive detector (INEL CPS 120) as detailed elsewhere [13]. The texture of such films is axially symmetric with the symmetry axis parallel to the film's normal [9]. It is then scanned only on the tilt angle (ρ, Fig. 1) (no azimuthal scanning) between 0°, to probe (*hkl*) planes parallel to the sample plane, and up to 70° for inclined planes, using a 5° step. Each diagram was acquired in 1800 s.

2.3. X-ray absorption spectroscopy

The Ni K edge absorption was recorded on the D42 station of the DCI ring in LURE. The samples were set in a holder allowing us to rotate it with respect to the synchrotron beam direction. Thus we record the absorption coefficients ($\chi(\alpha)$) for $\alpha = 70$, 60°, 50°, 35°, 20°, 0°, where α is defined according to Fig. 1. The $k\chi(k)$ function was extracted from the absorption coefficient with the software developed at LURE by Michalowicz [14], according to the procedure described in previous references [7,8]. Using the FEFF6 code [15], the EXAFS signal was calculated for the reference structures: $Ni(OH)_2$ [1] and $Ni_3Si_2O_5(OH)_4$ [16]. For the references, we have fixed the number of neighbours, N_i, for each shell and let refine the other parameters of the EXAFS equation (1):

[1] $Ni(OH)_2$ was obtained by hydrothermal treatment from Ni acetate tetrahydrate and sodium hydroxide. The X-ray diffraction pattern, recorded in the angular range 2–70° in 2θ with a 0.01° step for 20 s each step, was refined by the Rietveld method using Fullprof.

$$k\chi(k) = -S_o^2 \sum_i \frac{N_i}{R_i^2} |f_i(k,R_i)| e^{-2\sigma_i^2 k^2} e^{-2R_i/\lambda_i(k)} \times \sin(2kR_i + \phi_i(k,R_i)), \quad (1)$$

where i is the number of backscatterer shell, N_i the number of atoms at a distance R_i from the central Nickel atom for each shell, σ_i the Debye–Waller factor, λ_i the mean free path, ϕ_i and f_i the phase and amplitude for the ith backscatterer. S_o^2 is the reduction factor (fixed to 1).

The inverse Fourier transform of the first peak for the different α angles were fitted in order to evaluate the flattening angle of the Ni–O octahedra, β_O, β_{iu_j} being defined in Fig. 1. In these cases, N_O and R were allowed to be refined whereas the other parameters were fixed. An analogous procedure was used for the second peak in order to evaluate β_{Ni} and β_{Si}.

3. Results and discussion

3.1. Quantitative texture analysis [17]

Fig. 2 shows the variation with ρ of the 10–60° 2θ Bragg angle range. Clearly, the (00ℓ) lines decrease rapidly with increasing ρ. At $\rho = 30°$ no more signal from the (00ℓ) is visible, as a sign of a strong texture, with $\{00\ell\}$ planes parallel to the sample plane. The integrated $\{00\ell\}$ peaks have been fitted as gaussian shapes in 2θ. From the pole figures, the texture is quantified through the refinement of the orientation distribution function. Since this function tests for the compatibility of the crystallographic angles between lines, it becomes possible to dissociate the different indexing possibilities during the refinement. We operated several index combinations, taking into account several overlap possibilities, with a maximum of three reflections for each pole figure (each overlap). The following combinations were found to result in the best reliability of the ODF, for **S50**: $(005) = 100\%$; $[(22\bar{6})/(134)/(13\bar{7})] = [30\%/50\%/20\%]$; $[(22\bar{10})/(22\bar{11})/(22\bar{12})] = [25\%/25\%/50\%]$; $(2012) = 100\%$.

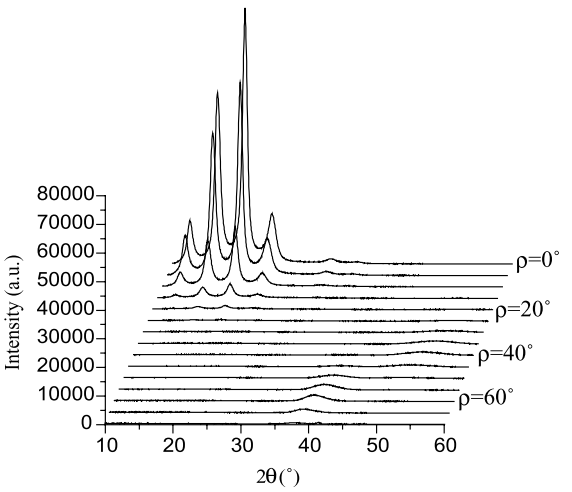

Fig. 2. ρ variation (from 0° to 70° by 5° step) of the diffractograms for sample **S50**.

Fig. 3 shows the experimental-normalised (incomplete) pole figures and the complete normalised pole figures as recalculated from the ODF. The texture is very strong, reaching maximum density values near 71 m.r.d in the fibre direction (centre of the $\{001\}$ pole figure), and a maximum ODF of 70.5 m.r.d. The associated quantities which attest for the texture strength are the entropy and the texture index. They reach values of

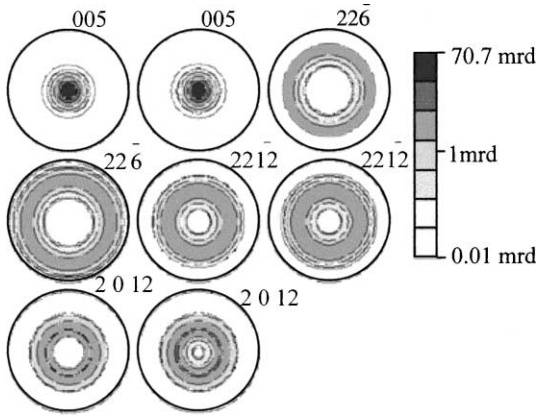

Fig. 3. Experimental-normalised pole figures and complete recalculated normalised pole figures for sample **S50**. Logarithmic density scale and equal area projections are used for the pole figures. $RP_0 = 7.7\%$ and $RP_1 = 3.7\%$ with $RP = (1/I) \times \sum_{hkl} \sum_j (P_{hkl}^{calc}(j) - P_{hkl}^{exp}(j))/P_{hkl}^{exp}(j)$, P_{hkl}^{exp} and P_{hkl}^{calc} corresponding to the experimental and calculated density poles, the summation on j is performed for the different ρ values, I is the number of measured poles.

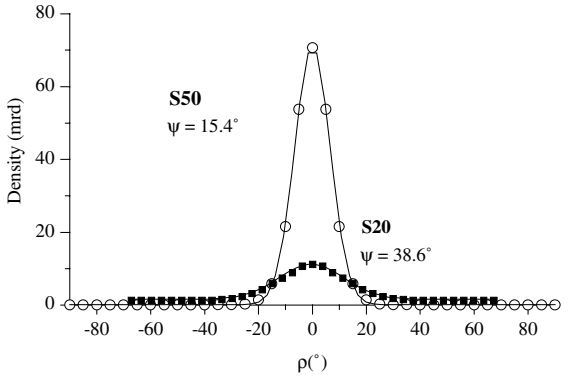

Fig. 4. Dispersion curves of the {0 0 1} pole figures for sample **S50** and **S20**.

−3.24 and 37.3 m.r.d^2 respectively, comparable to the strongest textures observed in phyllosilicate self-supporting films [12]. In Fig. 4, the dispersion curve of the {0 0 1} pole figure shows the radial dispersion of the crystallites relative to the film plane. This dispersion has a full width at half maximum (FWHM) of 15.4°, using a gaussian model. For the other sample, prepared in 20 ml water, a similar analysis has been performed. Compared to **S50**, less intensity is observed in the peaks and the decrease in intensity in ρ, looks smoother. It has been impossible to integrate lines different from the (00ℓ), and to get enough information to refine the ODF, because the orientation space is not fully covered by the experiment with as few lines. The radial distribution is consequently much larger than for **S50**, with 38.6° of FWHM, and the corresponding maximum of the distribution density smaller (13 m.r.d) (Fig. 4).

This study clearly demonstrates the higher orientation of **S50** sample. This compound exhibits a higher crystallinity and a lower organic content. Assuming the size and the surface charges of the colloids are driving the stacking of the platelets, it is expected that the sample exhibiting larger grains and less surface charges leads to the better textured film. Its maximum orientation density reaches a very high value, 70 m.r.d, compared to 39 m.r.d for nontronite [10], already mentioned as highly textured for a monoclinic self-supported film. The angular dispersion of our film S50 has a maximum value of 25° (Fig. 7) with a FWHM of 15.4°. This means that this sample is particularly adapted for P-EXAFS measurements to discriminate between in-plane and out-of-plane atom contributions. The other sample, **S20**, exhibits a texture comparable to the one of another natural nontronite [12] and is also suitable, for P-EXAFS.

3.2. Polarised EXAFS

In a few words (see [9–12] for more detailed explanations), the amplitude of EXAFS spectra depends on the angle between the electric field vector ($\boldsymbol{\varepsilon}$) of the incident beam and the vector linking the absorbing and backscattering atoms. P-EXAFS has therefore the possibility to probe layered structures for axisymmetrically oriented samples between two different directional limits, parallel and perpendicular to the (0 0 1) plane by varying the angle between the self supporting film and $\boldsymbol{\varepsilon}$. For instance, when the electric field of the incident beam is perpendicular to the film surface ($\alpha = 90°$) and thus to the layers, the contribution of the in-plane backscattering atoms is lowered with respect to the out-of-plane one. The experimental spectra are reported in Fig. 5 for **S50**, for the different incident angles. The strong dependence upon the incident beam angle is to be noticed. This angular dependence can be written as $\chi(\alpha) = \chi(0°)\cos^2\alpha + \chi(90°)\sin^2\alpha$ which leads to

$$\chi(\alpha) = \chi(90°) + (\chi(0°) - \chi(90°))\cos^2\alpha. \quad (2)$$

The 90° absorption can not be reached experimentally since the beam would have to be tangent to the film surface. Nevertheless it can be calculated from several angular spectra, by extrapolating equation (2). Therefore, the linear relationship between χ and $\cos^2\alpha$ has been checked. The correlation factor points out the goodness of the latter linear fit. For each k value, the ordinate at origin of χ versus $\cos^2\alpha$ leads to χ for $\alpha = 90°$. Using this procedure, it was possible to calculate the EXAFS spectra for $\alpha = 90°$, also reported in Fig. 5. Isosbestic points are evidenced by arrows on the previous curves. These points correspond to k values for which $\chi(k)$ is independent of α. For these particular k values, the correlation factor (r) for the linear regression is zero. Therefore we reported in Fig. 5 (upper curves), the r^2 factors which allow

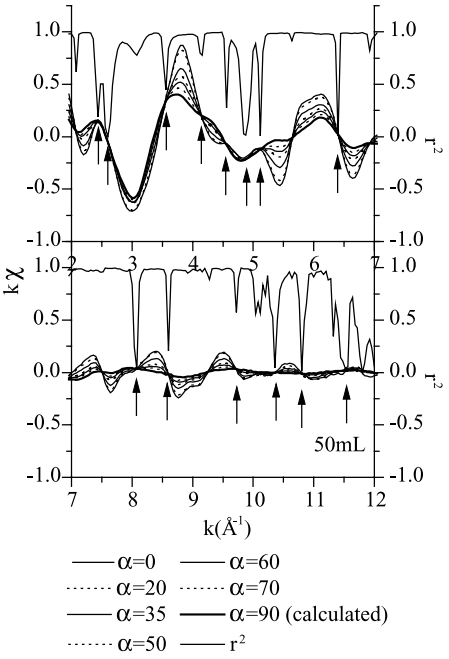

Fig. 5. $k\chi$ versus k for different experimental α and calculated for $\alpha = 90°$, for sample **S50**. Measurement of the absorption coefficients in transmission mode using air filled gas ionisation chambers, in the 8200–9300 eV energy range with a 5 eV step scan before the edge, 0.5 eV across and 2 eV after, using a 2 s accumulating time, Ni K-edge of a Ni metal slide as energy calibration, average on three signals for the best textured and 4 for the less one.

to locate the isosbestic points. It has to be noticed that the occurrence of these points is indicative of a correct extraction of the EXAFS from the absorption coefficients. Radial structure functions (RSF) obtained by Fourier transforms of the $k^3\chi$ spectra are shown in Fig. 6. A large dependence upon polarisation clearly appears. The contribution of the out-of-plane scattering atoms is lowered for spectra measured at lower α values, due to the texture of the sample and its layered structure. Six peaks (A, B, C, D, E and F) are observed on these curves. Calculations performed with FEFF6 based on the serpentine model were performed with polarisation along the layers ($\alpha = 0°$), perpendicularly ($\alpha = 90°$) or without (powder spectrum, corresponding to $\alpha = 35.3°$) in order to assign these peaks. As already mentioned [7,8], peak A corresponds to the first O, OH shell around Ni absorbing atom at distances of 2.05(2) Å

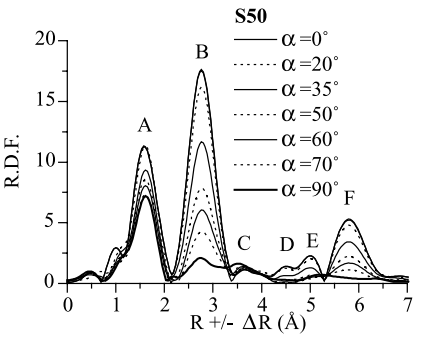

Fig. 6. FFT of the absorption coefficient performed on $k^3\chi$ for sample **S50**, with a Kaiser weighted window ($\tau = 2.5$) in the 2–12 Å^{-1} k-range.

and peak B was attributed in the same references to the contribution of nearest in-plane Ni atoms at $R = 3.11$ Å and of nearest out-of-plane Si atoms at $R = 3.24$ Å. Peaks D, E and F show the same α dependence with fast intensity decrease from $\alpha = 0°$ to $\alpha = 90°$. They correspond to Ni–O at 4.3 Å (D) and Ni–Ni at 5.3 Å (E) simple scattering and peak F arises from multiple scattering between Ni. The attribution of peak C is doubtful, its evolution with α is reverse than the other ones, indicating that it can be due to out-of-plane atoms. Moreover when considering the Fourier transform performed on $k\chi$, i.e. increasing the light element contribution, it appears that this peak is brought to the fore. This feature is an indication that oxygen or silicon out-of-plane atoms are concerned.

Finally, the octahedron flattening angle, β, could be estimated. It has already been demonstrated that for polarised EXAFS, the EXAFS oscillations are related to the powder contribution through [9]

$$\chi_{ij}^{P} = 3\chi_{ij}^{\mathrm{iso}} \sum_{u_j=1}^{N_j^{\mathrm{real}}} \cos^2\theta_{iu_j} = 3\langle \cos^2\theta_{iu_j}\rangle \chi_{ij}^{\mathrm{iso}}. \tag{3}$$

For layered compounds, the θ angle can be expressed from β and α and finally plotting the fitted apparent coordination versus $\cos^2\alpha$ leads to β,

$$N_j^{\mathrm{app}} = N_j^{\mathrm{real}}\left[1 - \frac{(3\cos^2\beta_j - 1)(3\cos^2\alpha - 2)}{2} I_{\mathrm{ord}}\right], \tag{4}$$

where N_j^{real} is the fitted coordination and I_{ord} accounts for the particle disorder. The I_{ord} values are evaluated from [18] to 0.82 and 0.96 for **S20** and **S50** respectively taking into account the texture.

Fitting of the inverse Fourier transform of the first peak corresponding to the 6 Ni–O distances of the brucite like layer was performed for different polarisation angles. As depicted in Fig. 7, plotting N_j^{app} versus $\cos^2\alpha$ allows us to check the linear variation between these two parameters. For $\alpha = 35.3°$, the coordination, N_j^{real}, is deduced from the fitting parameters to be 6.0 and 6.3 for samples **S20** and **S50** respectively, the β angle is 59.0 and 60.0° respectively. The accuracy on the latter can be estimated to 1°, no remarkable difference can be noted between both samples.

Such a procedure can also be applied to the second peak. An evaluation of the Ni–Ni and Ni–Si angles is possible. This was already done for Co adsorbed on clay [12]. In the same manner N_j^{app} versus $\cos^2\alpha$ is plotted for Ni–Ni and Ni–Si contributions (Fig. 7). As expected, an increase in N_j^{app} is observed with increasing $\cos^2\alpha$ for Ni second neighbours. This is related to the fact that when probing bounds parallel to the layer, the apparent coordination becomes greater. The real coordination can be calculated and is 5.6(1.0) and 5.7(1.0) for samples **S20** and **S50** respectively. The angle between Ni absorber and Ni backscatterer is evaluated to be 82° and 81°. Taking into account their precision these values are in agreement with Ni in trioctahedral layers: 6 Ni as second neighbours with a 90° angle with the normal. Concerning Si, a decrease in N^{app} was expected with increasing $\cos^2\alpha$, with the hypothesis that silicate species are grafted perpendicularly to the layers: β angles ranging from 22 to 40° depending on the phyllosilicates [19]. The N^{app} variation with $\cos^2\alpha$ is then expected to follow a linear dependence with a negative slope. As depicted in Fig. 7, N^{app} is almost constant, it is noticeable that for every α angle, a contribution close to 2 Si has to be accounted for to fit the signal coming from the inverse Fourier transform of the second peak. This means that whatever the incident beam orientation, Si is always present around Ni. However, the β angle that we can estimate is close to 60°:62° (**S20**) and 66° (**S50**). From the structural point of view, such an angle imposes that Si is very close to the layer. In this case, it is so close that the Ni–Si distance would be smaller than the fitted one. We propose that there is a wide distribution on the Ni–O–Si angles from ≈35° which correspond to O–Si bond perpendicular to the layer, to almost 90° when on the edge of the crystal Si species can be grafted parallel to the layers. Since the crystallites are small, the proportion of such Si can not be neglected. Moreover it has to be noticed that there is a great uncertainty on N_{Si} due to the fact that its contribution is hidden by the contribution of 6 heavy Ni atoms.

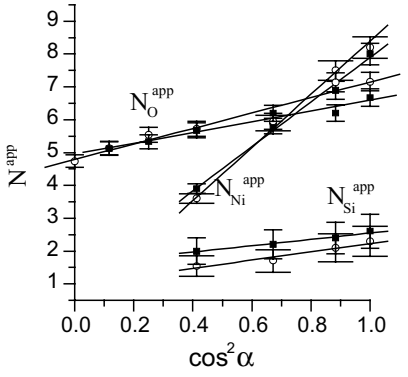

Fig. 7. Linear relation between apparent coordination and $\cos^2\alpha$ allowing one the determination of the β angles for Ni–O, Ni–Ni and Ni–Si. **S50**: $N_O^{app} = 4.82 + 2.31\cos^2\alpha$, $r^2 = 0.94$; $N_{Ni}^{app} = 0.28 + 8.10\cos^2\alpha$, $r^2 = 0.99$; $N_{Si}^{app} = 0.92 + 1.32\cos^2\alpha$, $r^2 = 0.97$; **S20:** $N_O^{app} = 4.95 + 1.64\cos^2\alpha$, $r^2 = 0.96$; $N_{Ni}^{app} = 1.11 + 6.77\cos^2\alpha$, $r^2 = 0.99$; $N_{Si}^{app} = 1.58 + 0.96\cos^2\alpha$, $r^2 = 0.98$.

4. Conclusion

P-EXAFS has been applied to two layered hybrid organic–inorganic silicates. The texture measurements reveal that the films are strongly textured especially for the sample containing less silicates and less organic species (**S50**). Varying the incidence angle of the synchrotron beam respectively to the films normal implies a strong dependence of the EXAFS oscillations indicating that different environments are probed around Ni during the experiments. Fitting the inverse Fourier transform of the first peak in the RSF for the different angles allows us to determine the flattening angle of the

octahedra around Ni^{2+}. The values are close for samples **S50** and **S20**. A similar procedure was carried out concerning the second peak of the RSF. Both samples are confirmed to be built up of trioctahedral layers, with 6 Ni at 3.10 Å and a β angle close to the 90° expected one. The main point of this study is related to the occurrence of a Ni–O–Si bond. In the case of clays, the Si tetrahedra are forming hexagonal rings by sharing corners. The β angle deduced from the variation of N^{app} with $\cos^2 \alpha$ is close to 60°. This means that such a geometry does not take place.

Lastly, the insight we got from the local Ni environment in both samples, is that there are no difference locally around the transition metal cation. Then the exchange interaction between Ni neighbours is similar in both samples. And actually, at high temperature the main feature in the magnetic behaviour is the presence of strong ferromagnetic interactions. The antiferromagnetic state observed at low temperature for sample **S50** is due to an antiferromagnetic coupling between ferromagnetically coupled Ni^{2+} layers, taking place at a great distance, via hydrogen bonds, through the organic species.

References

[1] N. Whilton, S. Burkett, S. Mann, J. Mater. Chem. 8 (8) (1998) 1927.
[2] M. da Fonseca, C. Airoldi, J. Chem. Soc. Dalton Trans. (1999) 3687.
[3] S. Burkett, A. Press, S. Mann, Chem. Mater. 9 (1997) 1071.
[4] M. da Fonseca, C.R. Silva, J.S. Barone, C. Airoldi, J. Mater. Chem. 10 (2000) 789.
[5] Y. Fukushima, M. Tani, Bull. Chem. Soc. Jpn. 69 (1996) 3667.
[6] M. da Fonseca, C. Silva, C. Airoldi, Langmuir 15 (1999) 5048.
[7] M. Guillot, M. Richard-Plouet, S. Vilminot, J. Mater. Chem. 12 (4) (2002) 851.
[8] M. Richard-Plouet, S. Vilminot, M. Guillot, M. Kurmoo, Chem. Mater. 14 (2002) 3829.
[9] A. Manceau, D. Chateigner, W.P. Gates, Phys. Chem. Min. 25 (1998) 347.
[10] M. Schlegel, A. Manceau, D. Chateigner, L. Charlet, J. Colloid. Interf. Sci. 215 (1999) 140.
[11] M. Schlegel, Thèse de l'Université Joseph Fourier, Grenoble I, 2000.
[12] A. Manceau, B. Lanson, V.A. Drits, D. Chateigner, W.P. Gates, J. Wu, D. Huo, J.W. Stucki, Am. Miner. 85 (1) (2000) 133.
[13] J. Ricote, D. Chateigner, G. Ripault, L. Pardo, M. Alguero, J. Mendiola, M.L. Calzada, in: J.A. Szpunar (Ed.), Textures of Materials, Vol. 2, NRC Research Press, Ottawa, 1999, p. 1327.
[14] A. Michalowicz, EXAFS pour le Mac, Logiciels pour la Chimie. Soc. Fr. Chim. (1991) 102.
[15] J.J. Rehr, J. Mustre de Leon, S.I. Zabinsky, R.C. Albers, J. Am. Chem. Soc. 113 (1991) 5135.
[16] S.H. Hall, S. Guggenheim, P. Moore, S.W. Bailey, Canad. Miner. 14 (1976) 314.
[17] A. Manceau, M. Schlegel, D. Chateigner, B. Lanson, C. Bartoli, W. Gates, in: D.G. Schulze, J.W. Stucki, P.M. Bertsch (Eds.), Synchrotron X-ray Methods in Clay Science, The Clays Minerals Society, 1999, p. 68.
[18] A. Manceau, M. Schlegel, Phys. Chem. Miner. 28 (1) (2001) 52.
[19] S.W. Bailey, in: P.H. Ribbe (Ed.), Hydrous Phyllosilicates, Vol. 19, Mineralogical Society of America, 1988.